Predominance of Nonequilibrium Dynamics in the Photodissociation of Ketene in the Triplet State†

Alexey L. Kaledin, Jeonghee Seong, and Keiji Morokuma*

Cherry L. Emerson Center for Scientific Computation and Department of Chemistry, Emory University, Atlanta, Georgia 30322

Received: October 16, 2000; In Final Form: January 26, 2001

The photodissociation of ketene is studied using direct surface-hopping classical trajectories where the energy and gradient are computed on the fly by means of state-averaged complete active space self-consistent field with a double-ζ polarized basis set. Three low-lying electronic states, singlets S_0 and S_1 and triplet T_1, are involved in the process of photodissociation of triplet state ketene. We propagated a trajectory, starting at the Franck−Condon geometry on S_1, and branched it out into many child trajectories every time the propagating potential energy surface (PES) crossed with another PES. The major photodissociation pathway to the triplet products was found to be $S_1 \rightarrow S_0 \rightarrow T_1 \rightarrow CH_2(X^3B_1) + CO(X^1\Sigma^+)$. It has been found that (1) the S_0-T_1 nonadiabatic transition creates the T_1 species nonstatistically at restricted regions of phase space and (2) a large fraction of the T_1 species thus created dissociates almost immediately, leaving no time for equilibration of internal degrees of freedom. Whether a specific T_1 trajectory dissociates fast or not is determined by the amount of C−C stretch vibration at the S_0-T_1 branch point. In essence, the above observations suggest strongly that the T_1 photodissociation process is highly nonstatistical, thus making equilibrium-based statistical theories inapplicable for computing the dissociation rate.

I. Introduction

Photodissociation of ketene in the first triplet state T_1 has intrigued experimentalists and theoreticians over the past few years.[1−8] Rate constants for the unimolecular decomposition of ketene were measured in the energy regime near the threshold for the triplet products, $CH_2(X^3B_1)$ and $CO(X^1\Sigma^+)$. Ketene was prepared in the ground electronic state S_0 and excited by a near-UV ($h\nu$ = 350 nm, 3.53 eV) laser pulse to the first excited singlet state S_1, intersystem-crossed to T_1, and dissociated into $CH_2(X)$ and CO. The rate constant for dissociation was observed to increase *stepwise* with increasing excitation energy and was interpreted reasonably well by the Rice−Ramsperger−Kassel−Marcus (RRKM)[9−12] theory, which predicted a similar stepwise shape.[2] However, a quantum dynamical calculation by Gezelter and Miller,[5] using vibrational frequencies for the exit barrier on T_1 computed by Allen and Schaefer,[4] revealed a rate constant increasing monotonically as a function of energy. The stepwise structure was destroyed by tunneling through the exit barrier. Gezelter and Miller suggested that the barrier frequency, which was 379*i* cm^{-1}, needed to be reduced by a factor of 4 to suppress the tunneling and thus recover the stepwise structure.

Such a large correction to the barrier frequency seemed unreasonable given the high level of ab initio theory used in the calculations. As a consequence, the statistical theory applied to T_1 was questioned and the role of nonadiabatic processes was proposed to be a significant factor in the photodissociation.[6] Cui and Morokuma investigated nonadiabatic interactions at the complete active space self-consistent field (CASSCF)[13] and the equation of motion coupled cluster (EOM-CCSD)[14] levels of theory. Seams of crossing among the S_0, S_1, T_1, and T_2 surfaces and associated matrix elements of spin−orbit coupling were calculated. Important structures, energies, imaginary frequencies, and coupling elements obtained by them are summarized in Figure 1. The authors suggested that S_1 and T_1 do not interact strongly due to the small spin−orbit coupling, and the direct $S_1 \rightarrow T_1$ intersystem crossing is unlikely due to the high energy of S_1-T_1 surface crossing and the small coupling element. It was shown, however, that the triplet state is likely to be formed via the two-step $S_1 \rightarrow S_0 \rightarrow T_1$ process, the first of which is the efficient internal conversion. They argue that, if the $S_0 \rightarrow T_1$ process is efficient at high energy, then T_1 may not have a statistical distribution and therefore the statistical theory may have to be abandoned and nonadiabatic effects need to be treated explicitly. Following that work, Yarkony analyzed the role of conical intersections in the internal conversion of the photo-excited ketene.[8] Barrierless paths were identified in the Franck−Condon (FC) region leading to the equilibrium geometry of S_1 and to the minimum energy point on the S_1-S_0 seam of crossing. These results were in qualitative agreement with the calculations of Cui and Morokuma.

Up to date, the dissociation of triplet ketene has been assumed a statistical process, governed by adiabatic dynamics on the T_1 surface. Several calculations used the appropriate methodology to calculate the rate of dissociation.[2,5] But in view of peculiar discrepancies of quantum dynamics with experiment, it has become worthwhile to search for the solution in a different direction. In the present work, we are motivated by the unanswered question of the origin of the stepwise structure in the dissociation rate and hope to obtain qualitative insights on the nature of the dissociation dynamics by simulating the photodissociation process using classical trajectories including nonadiabatic transitions. One of the main points we wish to address is whether the dissociation to the triplet channel is a statistical or nonstatistical process.

† Part of the special issue "William H. Miller Festschrift".

* To whom correspondence should be addressed. E-mail: morokuma@emory.edu.

10.1021/jp003794c CCC: $20.00
Published on Web 02/22/2001

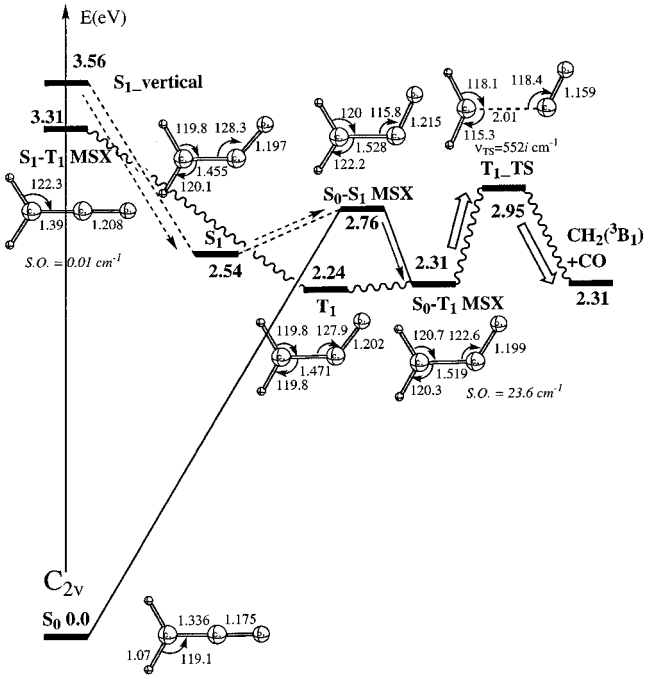

Figure 1. Potential energy profile of the three electronic states S_0 (solid line), S_1 (dashed line), and T_1 (wavy line) along the C−C reaction coordinate. The arrows map out the proposed dissociation pathway. The structures (Å and deg) and energetics are at the state-specific CASSCF/6-31G(d,p) level taken from ref 6.

II. Computational Methods

In the present study, ketene is initially assumed to be in the ground electronic state S_0 (X^1A_1 in C_{2v} symmetry). Upon excitation, the molecule accesses the first excited singlet state S_1 (A^1A_2) and then proceeds to decompose via two main pathways: (a) $S_1 \rightarrow S_0 \rightarrow T_1 \rightarrow CH_2(X^3B_1) + CO$; (b) $S_1 \rightarrow T_1 \rightarrow CH_2(X^3B_1) + CO$. We represent the dissociation by a single classical trajectory starting on S_1 at the equilibrium geometry of the ground state and a nonvibrating nonrotating molecular frame. The initial geometrical parameters are C−H = 1.069 Å, C−C = 1.336 Å, C−O = 1.182 Å, H−C−H = 122.2°, H−C−C = 118.9°, and C−C−O = 179.99°, as optimized for the ground-state minimum at the state-average CASSCF(10e/9MO)/6-31G(d,p) level, as discussed later. The slight distortion above in the C−C−O angle from 180° is created to produce an asymmetric gradient driving the system toward the C_s-II reaction path (see below). The trajectory is allowed to branch every time the potential energy surface (PES) on which the trajectory is propagated crosses another PES. At the branching point, the 'parent' trajectory continues to be propagated on the original PES, while the 'child' trajectory starts to evolve on the new PES. The nuclear momenta are not adjusted at the point of branch, since the energy of the two PESs is the same at this point. This technique is the well-known 'ants' surface-hopping trajectory method developed three decades ago by Tully and Preston.[15,16] Both the parent and the child trajectories are later assigned appropriate weights based on the electronic coupling element calculated or estimated a posteriori. The surface-hopping probability, or equivalently the weight, is calculated using the multidimensional version of the Landau−Zener formula.[17] A trajectory is declared finished when it either crosses a dividing surface for dissociation on T_1 or exceeds a reasonably large time limit. The dividing surface is a loose term in this context because we did not calculate the true reaction path. Our definition of the dividing surface is a point in the seven-dimensional space where the C−C bond distance becomes closest to 2.01 Å, the bond length at the T_1 transition state; this is the geometry where we analyze trajectories. We actually found that no trajectory we ran came back to the reactant side once it crossed the dividing surface. Allowing a large number of branches and propagating each branched trajectory for a significant interval of time, it should be possible to sample the important regions of the phase space as well as nonadiabatic transitions and make a qualitative understanding of the dissociation process.

All the trajectories were constrained to seven planar degrees of freedom in the C_s-II symmetry (for definitions see ref 6), i.e., confining all the atoms to lie in one plane and removing the two out-of-plane motions. The justification of the reduced dimensionality relies on the fact that the dissociation reaction path lies within C_s-II encompassing all the important stationary points along the way.[6−8,18] The Franck−Condon region, the minima on S_1, S_0, and T_1, the S_1−S_0 (conical intersection) and S_0−T_1 minima on the seams of crossing (MSX),[19] and finally the T_1 exit barrier, as shown in Figure 1, all lie within C_s-II. The role of the out-of-plane motion, as was argued by Cui and Morokuma,[6] is mainly to promote the S_1−S_0 internal conversion, which is known to be very efficient.

Newton's equations of motion were integrated in Cartesian coordinates by means of a second-order Taylor expansion, which requires the smallest number of expensive gradient evaluations calculated on the fly. Each subsequent step uses the information of the previous steps to predict the next positions and velocities. The integration step of 1 fs was chosen after a few test calculations showed a reasonable accuracy of the integrator, with an average relative error ϵ of the total energy (from S_0 minimum) of ∼0.1%. For some regions, especially at the point of branch, the error escalated to ∼0.5% but went down rapidly after a few steps. We made certain that the error did not accumulate during a run by scaling the atomic velocities by appropriate factors to conserve the total energy.

The energy and gradient needed for every step point of a trajectory were calculated using the state-average (sa) CASSCF method averaging the S_0, S_1, and T_1 states with equal weights. To make a meaningful comparison with our earlier work (ref 6), we used the same active space and basis set. The active space consisted of the valence electrons and orbitals excluding the oxygen 2s electrons and the two C−H bonds, thus putting 10 electrons into 9 molecular orbitals (MOs). The basis set used in the calculations was the standard 6-31G(d,p).[20] We note that in the earlier work, Cui and Morokuma used the state-specific CASSCF as opposed to the presently employed state-average CASSCF, which is responsible for small discrepancies in geometries and energies. The error in the relative energy (from S_0 minimum) between the two methods was observed to be ≤0.5%. The ab initio calculations were performed using the MOLPRO electronic structure code.[21]

III. Results of Trajectory Simulations

(A) The S_1 Trajectory and Its Branches. Figure 2 shows the S_1 trajectory along with snapshots of dynamically important structures. Velocity vectors (arrows at atoms) are also depicted to facilitate analysis. Inspecting the time profile of S_1 potential energy and the coordinates, one can see that the molecule is executing large amplitude C−C−H and C−C−O bending and C−C stretching vibrations around the S_1 minimum where ∠C−C−$H_{a,b}$ = 119.8° and 120.1° and ∠C−C−O = 128.3° (refer to Figure 1). In particular, the C−C excitation is created by the ∼0.11 Å lengthening of the C−C bond in the excited state S_1. On the other hand, the C−O and C−H stretches are not excited

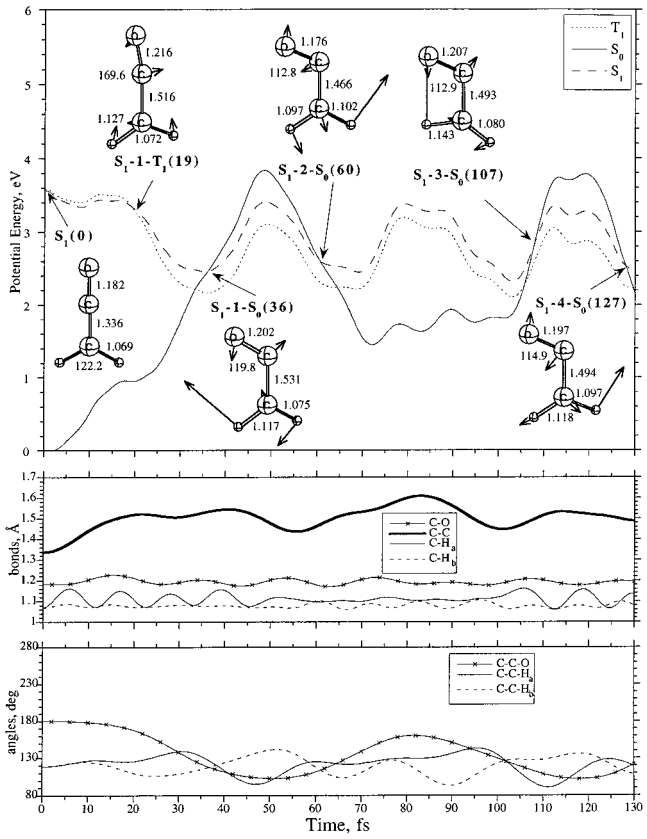

Figure 2. Trajectory propagating on the S_1 PES from the Franck−Condon geometry at $t = 0$. Potential energy of the propagating S_1 (long-dashed line) state, as well as S_0 (solid line) and T_1 (short-dashed line) states, bond distances, and bond angles as functions of the propagation time are shown. Arrows show S_1-1−T_1 and S_1-N−S_0 branch points, where branch trajectories are initiated on T_1 and S_0 states, respectively. The number in parentheses next to the structure label is time (fs) at the branching point. The structures at the branch points are shown with parameters (Å and deg); the velocity vector is also shown. The energy (eV) is with respect to the global minimum on S_0.

to a high degree in the process. It is interesting to point out that the two C−H stretch modes exchange energy as C−C−O swings back and forth.

As time progresses, the S_1 trajectory gives rise to several branches; in the span of 150 fs shown in Figure 2, a T_1 branch and four S_0 branches are created. The T_1 branch, denoted as S_1-1−T_1, starts just 19 fs after the photoexcitation. The system has not acquired much kinetic energy yet, and the C−C−O moiety is nearly linear. The location of the crossing point is in close proximity of the S_1−T_1 MSX (see Figure 1). Using the previously estimated spin−orbit coupling element of 0.01 cm^{-1}, the probability of surface hopping from S_1 to T_1 at this point is calculated at $\sim 2 \times 10^{-7}$. Although the spin−orbit element may not be very accurate because of the use of the one-electron effective spin−orbit Hamiltonian[22,23] for a light atom system, there is no doubt that the hopping probability is very small. We note that this is the only instance of S_1−T_1 crossing observed in the simulations, including the branched trajectories. This picture is quite rational considering that the S_1 and T_1 PESs, originating from the same electron configuration, go nearly parallel with each other, and their MSX lies high energetically (refer to Figure 1). After branching at S_1-1−T_1 at 19 fs, the T_1 trajectory (not shown in any figure) shows no signatures of dissociation up to 110 fs of propagation. Much like the parent S_1 trajectory, the H−C−C and C−C−O bends and the C−C stretch are appreciably excited while very little vibration is present in the C−O and C−H stretches. The S_1-1−T_1 trajectory crosses the S_0 PES with a regular frequency of once in 30 fs, with a mean hopping probability of $\sim 1.5 \times 10^{-7}$. In brief, the S_1−T_1 intersystem crossing appears a very unlikely event on counts of the weak electronic coupling as well as dynamical inaccessibility and is not likely to contribute to the photodissociation dynamics. This conclusion agrees with that deduced previously from the structure and energy of the S_1−T_1 MSX.[6]

Figure 2 also shows that the S_0 branches from the parent S_1 trajectory, labeled S_1-N−S_0 where $N = 1, 2, 3, 4, ...$, start at 36, 60, 107, 127, ... fs, regularly in 25−40 fs intervals, after the photoexcitation. Our earlier work suggested the probability of each hop at the conical interaction to be efficient.[6] The four branch structures in Figure 2 display the same trend; they are localized around the S_1−S_0 MSX, which is also very near the S_1 minimum (refer to Figure 1). The velocity vectors of two neighboring crossing points are similar in magnitude but approximately opposite in direction. As the molecule vibrates on the S_1 PES around its minimum, it samples the S_1−S_0 MSX on the incoming vibration (C−C−O bending inward) and on the outgoing vibration (C−C−O straightening). It takes a longer time to straighten than to bend owing to a strongly anharmonic S_1 potential. As a result, the crossing point pattern befalls in doublets which are separated by ~70 fs, and the time interval between two crossings in a doublet is ~25 fs. Since the S_1 trajectory does not have enough energy to dissociate adiabatically, it will vibrate regularly about the S_1 minimum giving rise to many S_0 branches. Indeed, the S_1−S_0 internal conversion appears to be a very efficient process in the present case, both electronically and dynamically.

(B) The S_1−S_0 Branches and Ensuing Dissociation on T_1. Propagating trajectories on S_0 branched at each of the S_1-N−S_0 branch points revealed very interesting dynamics. Figure 3 shows the details of the time evolution of the four trajectories: S_1-N−S_0, $N = 1, 2, 3, 4$, respectively. First of all, we observe that S_0 crosses T_1 (at S_0-Na−T_1 branch points) almost immediately after a branch took the system onto S_0, in a few femtoseconds at most. This is a reflection of the fact that the S_0−T_1 MSX has a structure similar to that of S_1−S_0 MSX. Consequently, the crossing structure and to a lesser degree the velocity vector are similar to the corresponding ones at the S_1-N−S_0 branch point. As we pointed out above, the branch structures are localized near the S_1 minimum and their vibrational motions essentially differ only in phase (C−C−O bending inward or straightening). Traveling on S_0 for a few femtoseconds before encountering T_1, however, changes the velocity quite noticeably but, most importantly, creates additional excitation along the C−C stretch. Inspecting the S_0-Na-T_1 branch points in Figure 3 demonstrates a large component of the velocity vector along the C−C bond for S_0-1a−T_1 and S_0-3a−T_1. On the other hand, S_0-2a−T_1 and S_0-4a−T_1 branch points have a much smaller velocity component along the C−C bond, but a very large component along the direction perpendicular to it. This difference will be discussed again later.

Another important observation in Figure 3 is that the S_0−T_1 crossings at later times (e.g. S_0-Nb−T_1 and S_0-Nc−T_1) exhibit crucial similarities to the S_0-Na−T_1 structures. All the later structures have very similar geometries, proving that the crossings are actually taking place near the S_0−T_1 MSX. In addition, some of these structures, e.g. S_0-1b−T_1, S_0-3a−T_1 and S_0-3c−T_1, also have large velocity components along the reaction coordinate, the C−C stretch. Estimating the probability of surface hopping based on spin−orbit coupling[6] and Laudau−Zener formula gives an estimate of the S_0−T_1 transfer to be

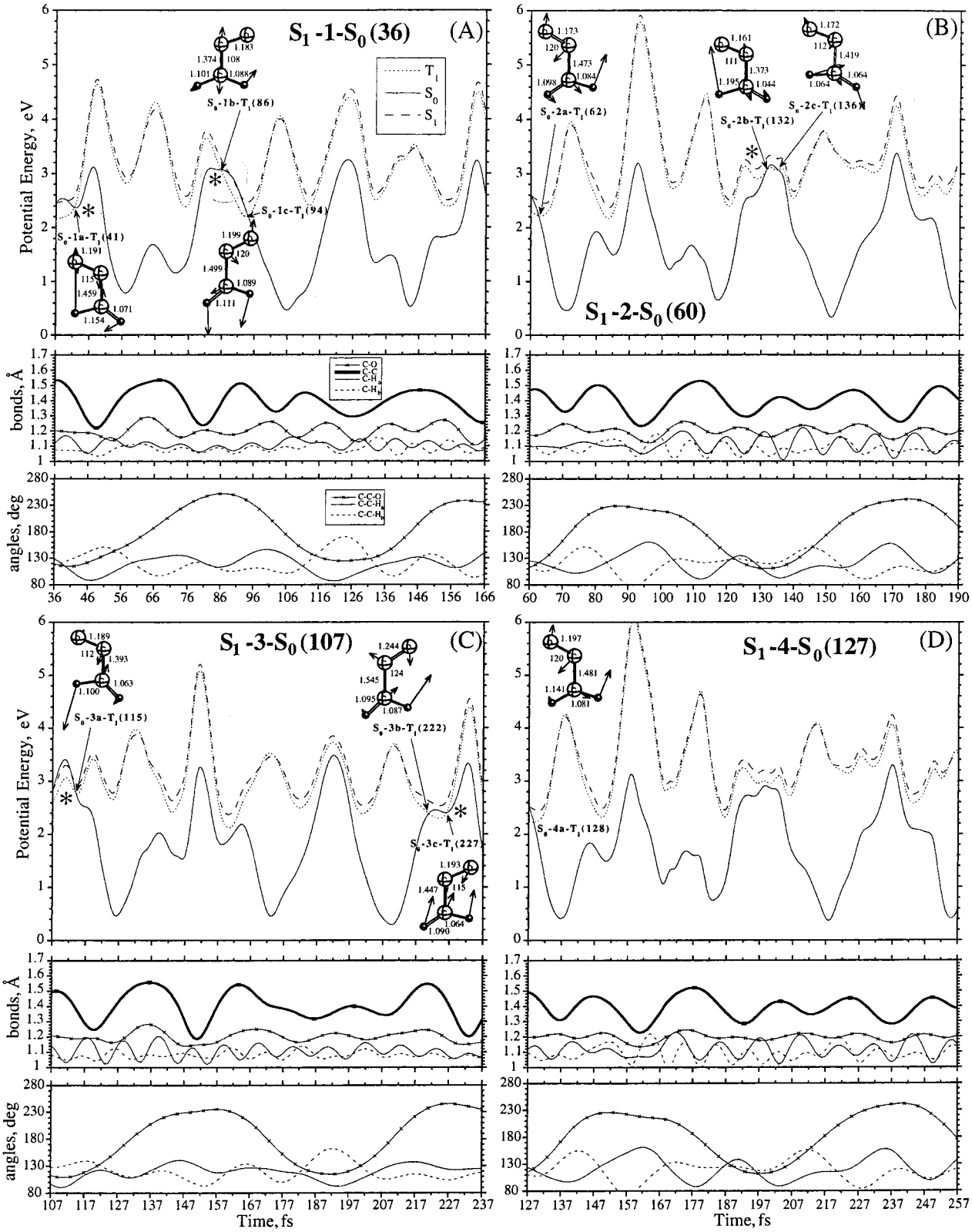

Figure 3. Four branched trajectories propagating on the S_0 PES, branching (A) at S_1-1−S_0 (36) branch point, (B) at S_1-2−S_0 (60), (C) at S_1-3−S_0 (107), and (D) starting at S_1-4−S_0 (127), with the time scale being continuous from the beginning of the S_1 trajectory in Figure 1. All the S_0-T_1 branch points are shown; those branch points which led to dissociation on T_1 are marked with an asterisk (*). The general labels are same as in Figure 2.

$\sim 10^{-5}$. This is 3 orders of magnitude less probable than the internal conversion, S_1-S_0, although it is 2 orders of magnitude stronger than the S_1-T_1 intersystem crossing ($\sim 10^{-7}$), which occurs early in the dissociation. And unlike the S_1-T_1 crossing, which was encountered only once and at a very early stage, the S_0-T_1 crossings are expected to take place repeatedly in more or less regular interval, as is seen in Figure 3, which would make the transfer even more efficient.

Finally, we propagated the 10 T_1 trajectories from the corresponding S_0-T_1 branch points. Although not shown for

TABLE 1: Average Geometry, Velocity, Speed (absolute value of velocity), and Their Standard Deviations at S_0-T_1 Branch Points and at the Dividing Surface on T_1

S_0-T_1	C−O	C−C	C−C−O	C−H_a	C−H_b	C−C−H_a	C−C−H_b
geometry (Å, deg)	1.190	1.443	115.7	1.114	1.074	115.2	115.7
Δ	0.022	0.055	4.9	0.035	0.014	13.4	9.7
velocity (Å,deg/ps)	−0.615	−7.690	0.997	−2.444	−1.167	−1.095	−0.209
Δ	6.718	23.315	2.084	24.170	12.638	2.872	1.698
speed (Å,deg/fs)	5.164	20.204	1.823	18.315	10.817	2.651	1.589
Δ	4.340	13.948	1.420	15.961	6.640	1.556	0.636
div surf	C−O	C−C ≈ 2	C−C−O	C−H_a	C−H_b	C−C−H_a	C−C−H_b
geometry (Å, deg)	1.142		135.4	1.115	1.080	125.6	108.3
Δ	0.016		8.9	0.023	0.004	3.6	9.8
velocity (Å,deg/ps)	−3.635	18.272	0.430	8.046	−0.186	−0.792	0.833
Δ	8.873	5.698	1.381	14.795	5.900	1.664	2.353
speedd (Å,deg/fs)	7.963	18.272	1.344	11.704	5.092	1.509	2.399
Δ	5.341	5.698	0.534	12.110	2.987	1.058	0.691

brevity, the T_1 trajectories starting at the branch points S_0-1*a*−T_1, S_0-1*b*−T_1, S_0-3*a*−T_1, and S_0-3*c*−T_1 dissociated promptly to $CH_2(^3B_1)$ + CO, taking on average 30 fs from the branch point to reach the dividing surface leading to the product. The S_0-2*b*−T_1 trajectory also dissociated but took 124 fs to do so (the C−C stretch at the crossing point is estimably smaller than in the other four reactive trajectories). The remaining five trajectories, S_0-1*c*−T_1, S_0-2*a*−T_1, S_0-2*c*−T_1, S_0-3*b*−T_1, and S_0-4*a*−T_1, did not dissociate after evolving on T_1 for 150 fs. The final rotation−vibration state distribution of the products of the five dissociated trajectories was not scrutinized closely, but a general trend of rotationally hot, vibrationally cold CO, and CH_2 excited in a combination of ν_2 and ν_3 modes was observed.

IV. Nature of the Dissociation Dynamics

(A) Equilibrium vs Fast Nonadiabatic Process. It was suggested in several experimental and theoretical studies that electronically nonadiabatic processes in ketene may play an important role in the outcome of the triplet dissociation products.[2,5,6,8] To reinforce this notion, we have shown that the only dynamically feasible pathway to the triplet products is via the $S_1 \rightarrow S_0 \rightarrow T_1$ channel. The direct $S_1 \rightarrow T_1$ channel can be safely disregarded owing to the combination of the small electronic and dynamical probabilities. The S_1-S_0 dynamics can be described as a very efficient (fast) process that leaves little time for the initial population of ketene to reach a thermal equilibrium in S_1. If we assume the probability of the S_1 to S_0 transition to be 10^{-2} (or larger) and the fact that the crossing occurs on average twice in pair every 70 fs, we calculate the classical lifetime of S_1 to be relatively short, about 3.5 ps. This is probably not long enough to equilibrate the available energy by distributing it into all the vibrational degrees of freedom.

The rate-determining step, as we have shown in the previous section, is the $S_0 \rightarrow T_1$ intersystem crossing. Yet even the relatively slow $S_0 \rightarrow T_1$ process does not prepare T_1 in an equilibrium state. Most importantly, the S_0-T_1 crossing point structures occur in a narrow range of phase space, as shown in Table 1 and illustrated in Figure 4. Table 1 shows the average structure, velocity, and absolute value of velocity with their standard deviations. Figure 4 illustrates these properties for the three coordinates that are most important for the dynamics: C−C and C−O stretches and C−C−O bend. Here we assumed equal weights for all structures in averaging over trajectories; proper averaging with electronic probabilities could be performed if statistically significant number of trajectories were available.

Very surprisingly, half the trajectories (5 out of 10) that hopped from S_0 to T_1 dissociated to the $CH_2(^3B_1)$ + CO products, most of them *almost immediately*, as summarized in the first two columns of Table 2. Those trajectories that led to dissociation, all have the fast-stretching C−C bond and the slowly varying C−O and C−C−O coordinates. Since the C−H and C−C−H coordinates are not coupled strongly to the reaction coordinate, the corresponding phase-space diagrams show much less structure than seen for those in Figure 4. The excitation of C−C stretch is expected, since the intramolecular forces between the C atoms are very different in S_1 and S_0, e.g. the C−C bonds are different by ∼0.11 Å at the corresponding equilibrium geometries. The remaining trajectories that showed no signs of dissociation had a much smaller velocity component along the C−C stretch at the moment of hop from S_0, cf. Figure 4. Obviously, the C−C vibration is the promotion mode; the high kinetic energy in this mode at the S_0-T_1 branching points enhances the probability of reaction. We find no clear evidence that the C−C−O bend, although highly excited throughout in all trajectories, helps promote the reaction.

(B) Specific Features of Dissociation in T_1. We now turn attention to dynamical behavior at the dividing surface. We have seen from our calculations that if a trajectory on T_1 reached such a geometry it never turned back and always proceeded to the CO + $CH_2(X^3B_1)$ products. The structures and velocity vectors of the aforementioned five reactive trajectories, as they crossed the dividing surface, are summarized in Figure 5, and the corresponding phase-space diagram is found in Figure 4. The lower part of Table 1 gives the average geometry, velocity, and speed and their deviations from average. The average geometry at which the molecule crosses over to the product side is similar to the T_1 transition state. In addition, only the C−C−O and one of the C−C−H angles deviate appreciably from the mean value. The velocity vector implies that the forming CO molecule will be rotationally excited. A simple impulsive model would also result in dissociation of some of the reactive trajectories. At the moment of the impulse (an S_0-T_1 branch point) the stretching C−C bond would drive the noninteracting CH_2 and CO partners apart and over the barrier. Judging by the velocity vectors, the resulting fragments would

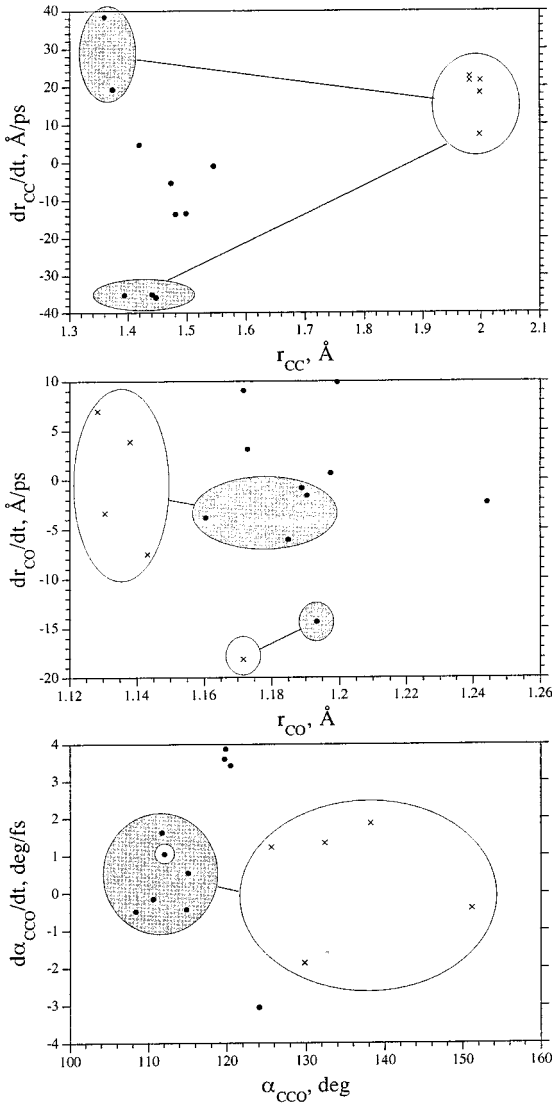

Figure 4. Phase-space diagrams for the C−C, C−O, and C−C−O coordinates. The dots are the geometries at S_0-T_1 branch points, and the crosses are the geometries at the dividing surface. Shaded ovals represent the dissociative regions of the S_0-T_1 phase space. Unshaded ovals represent the dividing surface.

TABLE 2: Total Time (from Franck−Condon Excitation) and Time on the T_1 PES Required To Reach the Dissociation Dividing Surface for Five Reactive Trajectories[a]

traj	total time (fs)	time on T_1 (fs)	$\cos^{-1}(\hat{v}\cdot\hat{s})$ (deg)	μ_s (m_p)	E_s (eV)	E_A (eV)	E_s/E_A (%)
1a	77	36	137.8	6.84	0.652	0.668	97.6
1b	108	22	80.2	7.22	0.044	0.743	5.9
2b	256	124	101.0	7.26	0.074	0.550	13.4
3a	150	35	86.5	6.98	0.005	0.361	1.4
3c	261	34	97.6	5.46	0.025	0.652	3.8

[a] Analysis of reaction coordinate at the dividing surface is also included, angle with velocity vector (deg), reduced mass (in proton mass), kinetic energy (eV), available energy (eV), and percent ratio (refer to text for explanation).

appear to have similar characteristics to the ones observed from actual calculations.

In a reduced dimensionality quantum calculation by Gezelter and Miller,[5] the CH_2 moiety was treated as a spherical particle. The approximation was made mainly for computational purposes even though it was known from earlier ab initio calculations[4] that CH_2 may be strongly coupled to the reaction coordinate.

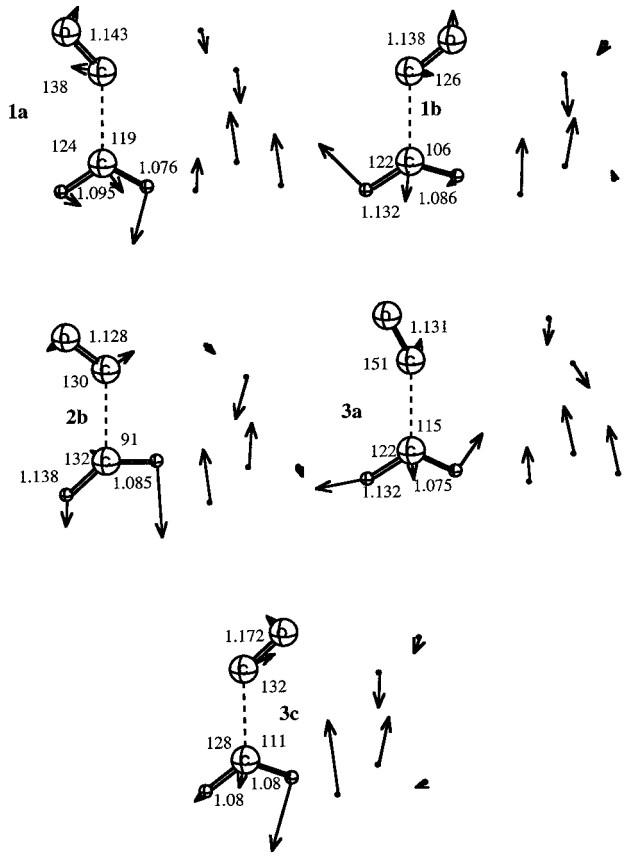

Figure 5. Structures (Å and deg) and velocity vectors of the five dissociative trajectories at the T_1 dissociation dividing surface. The reaction coordinate is shown to the right of each structure.

In the present trajectory calculations, we have not seen much evidence that any of the CH_2 modes influence the dissociation, i.e., reaching of crossing seams and excitation of the C−C stretch. The deviations in the C−H bonds and H−C−C angles are in good agreement with the high level ab initio calculations of King et. al.,[7] where it was shown that only the C−C distance and the C−C−O angle couple strongly to the reaction coordinate.

Finally, to address the question of later stages of the dissociation dynamics, we performed additional analysis at the dividing surface (cf. Table 2). Namely, we estimated the fraction of the kinetic energy in the reaction coordinate by projecting the velocity vector, $\vec{v}$, onto the harmonic normal coordinate, $\vec{s}$, with the imaginary frequency. The normal-mode analysis was performed for each structure in Figure 5. Of the five reactive trajectories, four behave similarly, having only a small fraction of kinetic energy in the reaction coordinate. They are **1b**, **2b**, **3a**, and **3c**. The average fraction of the reaction coordinate kinetic energy to the available energy is in the range of 1.4−13.4%. The remaining trajectory, **1a**, on the other hand, has nearly all of the available energy stored in the reaction coordinate, i.e., 97.6%. From the perspective of a transition-state theory (TST), the excess energy at the transition state is equipartitioned into the available degrees of freedom. In the present case, ∼15.3% should go into each of the six planar normal modes and about ∼7.7% should go into the kinetic energy along the reaction coordinate. While the four 'slow' trajectories behave more-or-less statistically, the 'fast' trajectory does not fall into the limits of a typical TST. Having only a few reactive trajectories, we cannot predict whether the reactive flux will be statistical or not, but we are definitely seeing

signatures of both 'fast' (nonstatistical) and 'slow' (statistical) reactive events.

V. Conclusions

By running a classical trajectory on the S_1 PES starting at the Franck−Condon structure and creating 'child' trajectories onto S_0 and T_1 at every branching point encountered, we obtained valuable insights into the photodissociation dynamics of triplet ketene following a photon excitation to S_1. The most important finding is that the dissociation process is rapid and very much nonstatistical. We have clearly seen that the channel that governs the dissociation is the $S_1 \rightarrow S_0 \rightarrow T_1$ surface coupling. The other proposed channel, namely the direct $S_1 \rightarrow T_1$ crossing, was shown to be not feasible. The following points outline the key features of our results: (i) the S_1-S_0 internal conversion is fast; (ii) the S_0-T_1 intersystem crossing occurs in a localized region of phase space; (iii) the ensuing T_1 dynamics yields rapid dissociation (∼30 fs) of half of the trajectories; (iv) the flux through the dividing surface is also localized to a narrow window in the phase space.

These findings make up a strong case against employing statistical theories to T_1 for calculating the unimolecular dissociation rate to the $CH_2(^3B_1) + CO$ products. The statistical theories assume an equilibrium distribution of all vibrational modes on T_1, which is not consistent with the localized S_0-T_1 surface-hopping dynamics and rapid dissociation on T_1.

Although we have demonstrated that surface hopping dominates the dissociation process, we cannot put definitive arguments on the *stepwise* shape of the unimolecular rate constant observed experimentally. The reason for the steps may still lie in the opening of quantum channels on the T_1 surface as the excitation energy is increased, but if the tunneling is somehow suppressed by the nonstatistical surface hopping and rapid dissociation, then the steps will not be washed out. The fact that as much as half of the trajectories that hopped to T_1 dissociated hints that tunneling may be a nonsignificant factor in the dissociation. To clearly answer the stepwise shape of the rate, it would be required to include quantization of energy in at least the S_0 and T_1 surfaces. Assuming that S_1-S_0 transition is fast and that S_0 reaches an equilibrium, one can run quantum wave packet or semiclassical dynamics on the coupled S_0 and T_1 surfaces. This is a part of our future plans on this problem.

Out present calculations are oversimplified in several aspects. We did not include the effect of noncoplanar motion, which will require full nine-dimensional dynamics. We assumed that the initial excited molecule had the S_0 equilibrium geometry; the full phase space of the initial zero-point vibration on S_0 should be sampled. We did not consider the energy dependence of the dynamics; the reaction probability needs to be calculated as a function of the excitation energy. And the effect of quantum dynamics, such as interference and tunneling, has not been taken into account. Obviously, more quantitative calculations are needed to answer many remaining questions on the triplet dissociation dynamics including the stepwise rate behavior.

Acknowledgment. The authors are extremely grateful to Prof. William H. Miller for stimulating discussions while he was a Visiting Fellow at the Emerson Center. Acknowledgment is also made to Dr. Qiang Cui for his early preliminary studies of the present system. This work was in part supported by Grants F49620-98-1-0063 and F49620-98-1-0345 from the Air Force Office of Scientific Research. Acknowledgment is also made for support of computing time at the Emerson Center of Emory University.

References and Notes

(1) Lovejoy, E. R.; Kim, S. K.; Moore, C. B. *Science* **1992**, *256*, 1541.
(2) Kim, S. R.; Lovejoy, E. R.; Moore, C. B. *J. Chem. Phys.* **1995**, *102*, 3202.
(3) Morgan, C. C.; Drabbles, M.; Wodtke, A. M. *J. Chem. Phys.* **1996**, *105*, 4550.
(4) Allen, W. D.; Schaefer, H. F., III. *J. Chem. Phys.* **1988**, *89*, 329.
(5) Gezelter, J. D.; Miller W. H. *J. Chem. Phys.* **1996**, *104*, 3546.
(6) Cui, Q.; Morokuma, K. *J. Chem. Phys.* **1997**, *107*, 4951.
(7) King, R. A.; Allen, W. D.; Ma, B.; Schaefer, H. F., III. *Faraday Discuss.* **1998**, *110*, 23.
(8) Yarkony, R. D. *J. Phys. Chem. A* **1999**, *103*, 6658.
(9) Rice, O. K.; Ramsperger, H. C. *J. Am. Chem. Soc.* **1928**, *50*, 617.
(10) Kassel, S. *J. Phys. Chem.* **1928**, *32*, 1065.
(11) Markus, R. A.; Rice, O. K. *J. Phys. Colloid. Chem.* **1951**, *55*, 894.
(12) Marcus, R. A. *J. Chem. Phys.* **1952**, *20*, 359.
(13) Werner, H.-J.; Knowles, P. J. *J. Chem. Phys.* **1985**, *82*, 5053.
(14) Stanton, J. F.; Bartlett, R. J. *J. Chem. Phys.* **1993**, *98*, 7029.
(15) Preston, R. K.; Tully, J. C. *J. Chem. Phys.* **1971**, *54*, 4297.
(16) Tully, J. C.; Preston, R. K. *J. Chem. Phys.* **1971**, *55*, 562.
(17) Chapman, S. *Adv. Chem. Phys.* **1992**, *82*, 423.
(18) Yamabe, S.; Morokuma, K. *J. Am. Chem. Soc.* **1978**, *100*, 7551.
(19) Kato, K.; Jaffe, R. L.; Komornicki, A.; Morokuma, K. *J. Chem. Phys.* **1983**, *78*, 4567.
(20) Hariharan, P. C.; Pople, J. A. *Mol. Phys.* **1971**, *27*, 209.
(21) Knowles, P. J.; Werner, H.-J. MOLPRO; University of Birmingham: U.K., 2000.
(22) Hess, B. A.; Marian, C. M.; Peyerimhoff, S. D. In *Modern Electronic Structure Theory I*; Yarkony, D. R., Ed.; Uto-Print: Singapore, 1995.
(23) Koseki, S.; Schmidt, M. W.; Gordon, M. S. *J. Phys. Chem.* **1992**, *96*, 10768.